

Osti

NINETH TECHNICAL PROGRESS REPORT
ON
HYDRODYNAMIC MODELS FOR SLURRY BUBBLE
COLUMN REACTORS

OCTOBER 1996

U.S. DEPARTMENT OF ENERGY GRANT
DE-FG22-94PC94028
208

DIMITRI GIDASPOW
PRINCIPAL INVESTIGATOR
DEPARTMENT OF CHEMICAL AND ENVIRONMENTAL ENGINEERING
ILLINOIS INSTITUTE OF TECHNOLOGY

U.S. DOE PATENT CLEARANCE NOT REQUIRED PRIOR
TO PUBLICATION OF THIS REPORT

RECEIVED
MAY 31 2000
OSTI

RECEIVED
USDOE/PETC
56 OCT 30 PM 2:34
ACQUISITION & ASSISTANCE DIV.

DISCLAIMER

This report was prepared as an account of work sponsored by an agency of the United States Government. Neither the United States Government nor any agency thereof, nor any of their employees, make any warranty, express or implied, or assumes any legal liability or responsibility for the accuracy, completeness, or usefulness of any information, apparatus, product, or process disclosed, or represents that its use would not infringe privately owned rights. Reference herein to any specific commercial product, process, or service by trade name, trademark, manufacturer, or otherwise does not necessarily constitute or imply its endorsement, recommendation, or favoring by the United States Government or any agency thereof. The views and opinions of authors expressed herein do not necessarily state or reflect those of the United States Government or any agency thereof.

DISCLAIMER

Portions of this document may be illegible in electronic image products. Images are produced from the best available original document.

ABSTRACT

HYDRODYNAMIC MODELS FOR SLURRY BUBBLE COLUMN REACTORS

The objective of this investigation is to convert our "learning gas - solid - liquid" fluidization model into a predictive design model. The IIT hydrodynamic model computes the phase velocities and the volume fractions of gas, liquid and particulate phases. Model verification involves a comparison of these computed velocities and volume fractions to experimental values.

As promised in the SIXTH TECHNICAL PROGRESS REPORT, January 1996, this report presents our measurements of radial distribution function for 450 micron glass particles in our liquid-solid fluidized bed. The report is in the form of a preliminary paper. We need the radial distribution function to compute the viscosity and the equation of state for particles. The principal results are as follows:

1. The measured radial distribution function, g_0 , is a monotonic function of the solid volume fraction. The values of the radial distribution function g_0 are in the range of the predictions from Bagnold equation and Carnahan & Starling equation.
2. The position of the first peak of the radial distribution function does not lie at $r = d$ at contact (d is particle diameter). This differs from the predictions from the hard sphere model and the measurements in the gas-solid system (Gidaspow & Huilin, 1996). This is due to a liquid film lubrication effect in the liquid-solid system.

Radial Distribution Function Measurements In A Liquid-Solid Fluidized Bed

Principal Investigator: Dimitri Gidaspow
Research Associate: Lu Huilin

Department of Chemical and Environmental Engineering
Illinois Institute of Technology
Chicago, IL. 60616

I. Introduction

In the computer simulations of the gas-solid, gas-solid-liquid systems, using codes such as FLUENT, FLUFIX, the viscosity of the particulate phase was needed as the input data (Gidaspow, 1994; Sinclair & Jackson, 1989; Pita & Sandaresan, 1991; Samuelsberg & Hjertager, 1996). Such measured viscosity data are scarce (Schuegel, 1971; Grace, 1982; Chen et al., 1994). Miller and Gidaspow (1992) obtained the particulate viscosity from a pressure-drop balance in which the particle flux was measured by an extraction probe and solid volume fraction by an X-ray densitometer. The prediction equation of the particulate viscosity, based on the kinetic theory of granular flow, needs the values of the radial distribution function.

An extensive literature on the radial distribution function is concerned with both the experimental prediction (Brown et al., 1976) and theoretical prediction. The radial distribution function defines the probability of finding a second particle at some position relative to a first particle located at the origin. The simplest intermolecular potential energy function that can be used to determine the thermodynamic properties is the hard-sphere model. The radial distribution function for this model has been theoretical determined both by analytical approaches (Thiele, 1963; Wertheim, 1963; Lebowitz, 1964; Baxter, 1968; Danning & Ahmadi, 1986) and by numerical methods (Alder & Hoover, 1968; Wood, 1968) involving Monte Carlo methods and molecular dynamics calculation. Carnahan & Starling (1969) proposed a semi-empirical equation of state from which they obtained the radial distribution function at contact for single-component of hard-sphere. It can be written in terms of the solid volume fraction ε_s as

$$g_0 = \frac{1}{1-\varepsilon_s} + \frac{3\varepsilon_s}{2(1-\varepsilon_s)} + \frac{\varepsilon_s^2}{2(1-\varepsilon_s)^3} \quad (1)$$

Their expression is in almost exact agreement with the "exact" numerical molecular dynamics calculations for value of ε_s up to about 0.5. But above this it gives g_0 that are

too low. Danning & Ahamdi (1986) developed a general expression for the equation of state to overcome this deficiency at the high solid volume fraction as follows:

$$g_0 = \frac{1 + 2.5\varepsilon_s + 4.5904\varepsilon_s^2 + 4.515439\varepsilon_s^3}{\left[1 - \left(\frac{\varepsilon_s}{\varepsilon_{s,m}}\right)^3\right]^{0.678021}} \quad (2)$$

where $\varepsilon_{s,m}$ is the maximum possible random close-pack volume fraction. Comparing Eq. (1) and (2), it was found that both equations have a significance difference only at the solid volume fraction larger than 0.57.

We define s as the mean separation between particles, then the $(s+d)$ is the mean distance between centers. The liner concentration is (d/s) . It is related to the linear radial distribution function g_0 by means of the following relation (Bagnold, 1954):

$$g_0 = \frac{s+d}{s} = \frac{1}{\left[1 - \left(\frac{\varepsilon_s}{\varepsilon_{s,m}}\right)^3\right]} \quad (3)$$

It can be seen that when the solid volume fraction approaches the random-packed volume fraction, the radial distribution function becomes infinity. The values from Eq. (3) are much higher than that of Eq. (1) and (2).

Several investigations have been undertaken to measure the liquid-solid suspension microstructure. Three particularly valuable techniques are as follows: X-ray diffraction, inelastic scattering of thermal neutrons, and laser-light scattering. The feature of X-ray scattering experiments is the fact that the energy of the incident radiation is much greater than the thermal energies of the objective and the scattering is elastic. In the case of thermal neutrons, the scattering cross-section can be measured as a function of energy transfer as well as momentum transfer. Hence this is an extremely powerful method of studying microscopic time-dependent processes. Direct observation by fluorescence microscopy and quasielastic light-scattering measurement to study particle distribution in polymer latex suspension have been carried out (Yoshida et al., 1990). Radial distribution functions were determined by measuring interparticle distances on the images.

Until now, there were no reliable data on the radial distribution function for large particle suspensions. The liquid-glass particle suspension was investigated in this study. The hydrodynamic behavior of particles was measured by our CCD camera technique.

II. Experimental Apparatus

The experimental apparatus is shown schematically in Fig. 1. Total height of the bed was 1.8 m with a 1.2 m height test section, and cross-section was 30.48 cm by 5.0

cm. The liquid enters the bed through a pipe-type distributor which contains 42 holes of 4 mm diameter and a perforated plate. Water was circulated by a centrifugal pump and through a surge tank. The fluxrate of water was regulated and measured using a calibrated rotameter. All liquid velocities mentioned in this article refer to the superficial velocities unless otherwise noted.

Glass particles with average diameter of 450 micron and density of 2600 kg/m³ were used as the solid phase. The static height in this study was kept constant at 20 cm from the perforated plate.

The microstructure of the liquid-glass suspension was investigated using the High Resolution Micro-Imaging/Measuring System (Gidaspow & Huilin, 1996). It was first used by Bahary (1994) and Gidaspow, Bahary and Wu (1995) for measurements in a three phase fluidized bed. The system consists essentially of two units: a high resolution micro-image system and a data manage system, see Fig. 1. The high resolution micro-image system is a 2/3 inch color video camera (DXC-151A) which uses a Charge Coupled Device (CCD), a solid stage sensor. This camera has ten electronic shutter settings and four modes for gain control. The horizontal resolution of the camera is 460 TV line, and a sensitivity of 2000 lux at 0 dB for gain. The camera adaptor is a Sony CMA-D2. The captured images were stored at a personal computer which has a Micro-Imaging Board and a Micro-Imaging software, Image-Pro Plus. These images were treated for further study.

Fig. 2 shows a typical captured and digitized image for 450 micron glass particles in a liquid-solid fluidized bed. The centers of each circle correspond to the projection of the centers of the particles. Thus a single image provides the two-dimensional particle distribution. The position and area of each particle was determined by software IPPLUS and stored in a PC computer.

III. Concept of Radial Distribution Function

The radial distribution function defines the probability of finding a second particle at some position relative to a first particle located at the origin. For a homogenous system, the n-particle distribution function $g_N^{(n)}(r^n)$ is defined in terms of the corresponding particle density as follows:

$$g_N^{(n)}(r^n) = \frac{\rho_N^{(n)}(r^n)}{\rho^n} \quad (4)$$

If the system is isotropic, the pair distribution function $g_N^{(2)}(r_1, r_2)$ is a function only of the separation $r_{12} = r_1 - r_2$, it is then usually called the radial distribution function

$g(r)$. From the particle coordinate distribution, the radial distribution function $g(r)$ was calculated as follows (Balucani & Zoppi 1994; Egelstaff 1967; Hunter 1989):

$$\Delta N = 2\pi\bar{r} \frac{N}{\text{AREA}} g(\bar{r}) \Delta r \quad (5)$$

where N is the total particle number in the AREA, and ΔN is the particle number in the computing area. Fig. 3 summarized the concept of the radial distribution function and its calculation. This method is very similar to the Monte Carlo simulation of the equation of state (Temporally et al. 1968; Beveridge et al., 1983). The "termination effect" was eliminated by the method described by Yoshida et al. (1990).

IV. Results and Analysis

A. Microstructure of Liquid-Glass Suspension

A typical image, Fig. 2 taken at instantaneous time, shows the views of particle distribution, and reveals some interesting features. It is clear that particle microstructure distribution is nonhomogeneous. A porosity structure coexists with disordered particles. We see coexistence of particles and liquid holes which are bubble-like as the gas-solid fluidization. Amazingly, the size of the holes is larger than 4 mm in diameter. This value is similar to bubble size in the gas-solid fluidized beds. Needless to say, these holes will effect the heat, mass transfer and reactions. Such structure nonhomogenties are important for understanding of dispersions.

B. Radial Distribution Function

Fig. 4 a, b, c and d show the measured radial distribution functions. The first peak of the radial distribution function represents the nearest neighbors. At higher values of (r/d) , there are oscillations representing more distant neighbors. These oscillations decrease in amplitude with increasing (r/d) , and eventually approach the mean density of the suspension. The peak intensity becomes higher with increasing particle volume fraction. This trend is in accordance with numerous scattering data not only in the latex system (Snook & Megen, 1976) but also in the ion polymer system (Ise et al., 1986).

Fig. 5 shows the comparison the experimental data with computed results as a function of solid volume fraction using Bagnold equation (3) and Carnahan & Starling equation (1). The solid volume fraction was measured using a method by Fan et al. (1985). We see that the measured radial distribution function is higher than the values calculated by Carnahan & Starling's equation, but smaller than that of Bagnold's equation.

C. Structure Factor

The radial distribution function can be transformed to the structure factor $S(k)$ by the inverse Fourier transfer numerically as follows (Egelstaff, 1967; Yoshida et al., 1990; Balucani & Zoppi, 1994):

$$s(k) = 1 + \rho_s \int [g(r) - 1] e^{ikr} dr \quad (6)$$

where k is the 'wave' factor. At higher values of k , Structure factor $s(k)$ oscillates, and for $k \rightarrow \infty$, The oscillations damp completely. Fig. 6 shows the structure factor profiles from the measured radial distribution function. The first peak reflects the existence of a dominant nearly regular arrangement of the particles in real space. At large 'wave' factor, the structure factor $s(k)$ approaches unity. At the opposite extreme, at 'wave' factor $k \rightarrow 0$, the structure factor $s(0)$ represents the macroscopic property of the system. This quantity which is related to the isothermal compressibility is defined as (Balucni & Zoppi, 1994, Hunter, 1989):

$$s(0) = m\theta \left(\frac{\partial \rho}{\partial P} \right)_T \quad (7)$$

where θ is the granular temperature which is analogous to thermal temperature. Fig. 7 shows the profile of the structure factor $s(0)$ with solid volume fraction. As far as the peak and the number of peaks are concerned, this fact implies that, even when broad scattering peaks as shown in Fig. 6 have been observed, we must admit the existence of a disordered structure or at least the coexistence of order structure and disordered regions in this liquid-glass fluidization system. Fig. 8 shows the profile of the major peak with solid volume fraction. Generally speaking, with decreasing solid volume fraction, the particle structure was more ordered in this system.

D. Mean Force

The mean force acting on particle 1 at position r_1 can be expressed in terms of radial distribution function (Hunter, 1989):

$$F_m(r) = \frac{m\theta}{g(r)} \frac{\partial g(r)}{\partial r_1} \quad (8)$$

where $F_m(r)$ is the mean force needed to move two particles through a liquid from some initial large separation to a separation r . In a dilute gas, this is just the work done against the interaction potential between two molecules. Fig. 9 shows the profile of the mean force. It can be seen that when $r \rightarrow \infty$ the fluctuations damp completely. Fig. 10 shows the minimum mean force (First lower peak) with solid volume fraction. As solid volume fraction increases, the mean force decreases.

E. Potential of Mean Force

The potential of mean force, analogous to the molecular theory, is defined as follow (Egelstaff, 1967):

$$F_p = m\theta \times \ln g(r) \quad (9)$$

where F_p is the potential of mean force which gives the normalized average force on particle 1 if particle 2 held fixed at \bar{r} . Fig. 11 shows the potential of mean force distribution. As the particles approach, the potential of mean force becomes more and more negative. Once the particles are separated by a distance less than the minimum in the potential of mean force, the potential of mean force becomes positive. These curves are very similar to molecular theory. When distance $r \rightarrow \infty$, the potential of mean force approaches zero. Fig. 12 shows the minimum potential of mean force with solid volume fraction. The depths of well are less than about $2m\theta$.

V. Discussion

From figure 4, we see that the closest interparticle distance shifts from the position of $r=d$ (d is the particle diameter). This distance should be at the position of $r=d$ in the theoretical simulation for one-component system. These values, however, are larger, near $1.5d$, in this study. According to hydrodynamics of film thinning, if s is the distance between two particle centers, and $D=s-d$ is the net distance, the hydrodynamic force between the particle surface due to viscous dissipation is (Hunter, 1989):

$$F_v = -\frac{3\pi\mu_f d^2}{2D} \frac{dD}{dt} \quad (10)$$

where μ_f is liquid viscosity. Note that $F_v > 0$ corresponds to a repulsive force. It is interesting to note that in Eq. (10) the hydrodynamic force becomes larger and larger when two particles attract, the lubrication of liquid film obstructs particle contact. The hydrodynamic force is proportional to liquid viscosity and particle diameter square. These effects therefore become dominant for large particles and high viscosity fluids. These influences cause the closest interparticle distance to shift to high values.

VI. Conclusion

In this study, the microstructure of particle distribution was carried out using our CCD camera technique in a liquid-glass particle fluidized bed. The coexistence of particles and liquid holes was found from the images. The properties of these liquid holes are very similar to gas bubbles in the gas-solid fluidized beds. The radial distribution function was determined directly from the particle coordinates in the two-dimensional images. The experimental data are larger than of Carnahan & Starling theoretical predictions, but smaller than those given by the Bagnold equation.

The structure factor using the inverse Fourier transform reveals that the liquid-glass suspension system in this study is disordered, and that there is a coexistence of ordered and disordered regions. The mean force, like in the molecular theory, shows that the energy needed to push two particles apart is about $2m\theta$.

Reference:

1. Alder B. J. & Hoover W. G., Numerical Statistical Mechanics, **Physics of Simple Liquids**, Edited by H. N. V. Temperally, J. S. Rowlinson & G. S. Rushbrooke, North Holland, 1968.
2. Bagnold R. A., Experiments on a gravity-free dispersion of large solid spheres in a Newtonian fluid under shear, *Proc. Roy. Soc.*, **A225**, 49-63, 1954.
3. Bahary M., Experimental and computational studies of hydrodynamics in two-and three phase fluidized beds, Ph. D. Thesis, IIT, 1994.
4. Balucani U. & Zoppi M., **Dynamics of The Liquid State**, Oxford Science Publications, 1994.
5. Baxter R. J., Percus-Yevick equation for hard spheres with surface adhesion, *J. Chem. Phys.*, **49**, 2770-2774, 1968.
6. Beveridge D. L., M. Mezei, P. K. Mehrotra, F. T. Marchese, G. Ravi-Shanker, T. Vasu and S. Swaminathan, Monte Carlo computer simulation studies of the equilibrium properties and structure of liquid water, **Molecular-based Study of Fluid**, Edited by J. M. Haile & G. A. Mansoori, American Chemical Society, 1983.
7. Brown J. C., J. W. Goodwin, R. H. Ottewill & P. N. Pusey, The determination of the radial distribution function for interacting latex particles. **Colloid and Interface Science IV**, Hydrosols and Rheology, Edited by M. Kerker, Academic Press Inc., 1976.
8. Carnahan N. F. & K. E. Starling, Equation of state for non-attracting rigid spheres, *J. Chem. Phys.*, **51**, 635-636, 1969.
9. Chen J. C., Polashenski W. and Tuzla K., Normal solid stress in fluidized beds, 1994 Annual Meeting of The American Institute of Chemical Engineers, Preprint Volume for Fluidization and Fluid-Particle Systems, November 13-18, San Francisco, California, 14-18. 1994.
10. Danning M. & G. Ahmadi, An equation of state for dense rigid sphere gases, *J. Chem. Phys.*, **84**, 3449-3450, 1986.
11. Egelstaff P. A., **An Introduction to The Liquid State**, Academic Press, 1967.

12. Fan L. -S, T. Kawamura, D. C. Chitester & R. M. Kornosky, Experimental observation of nonhomogeneity in a liquid-solid fluidized bed of small particles, *Chem. Eng. Commun.*, **37**, 141-157, 1985.
13. Hunter R. J., **Foundation of Colloid Science II**, Oxford Science Publications, Calarendon Press, 1989.
14. Ise N., T. Okubo, M. Sugimura, K. Ito & H. J. Noite, Order structure in dilute solutions of highly charged polymer lattices as studied by microscopy I. Interparticle distance as a function of latex concentration, *J. Chem. Phys.*, **78**, 536-540, 1983.
15. Gidaspow D., **Multiphase Flow and Fluidization, Continuum and Kinetic Theory Descriptions**, Academic Press Inc., 1994.
16. Gidaspow D., Bahary M. and Wu Y., Slurry bubble column reactor models using kinetic theory, 1995 Annual Meeting of The American Institute of Chemical Engineers, Preprint Volume for Fluidization and Fluid-Particle Systems, November 12-17, Miami Beach, 164-168, 1995.
17. Gidaspow D. & L. Huilin, Collisional viscosity of FCC particles in a CFB, *AIChE J.*, **42**, 2503-2510, 1996.
18. Grace J. R., Fluidized-bed hydrodynamics, **Handbook of Multiphase Systems**, Edited by G. Hetsroni, Hemisphere, 1982.
19. Lebowitz J. L., Exact solution of generalized Percus-Yevick equation for mixture of hard spheres, *Phy. Rev.*, **A133**, 895-899, 1964.
20. Miller A. and Gidaspow D., Dense, vertical gas-solid flow in a pipe, *AIChE J.*, **38**, 1801-1815, 1992.
21. Pita J. and S. Sandareasan, Gas-solid flow in vertical tubes, *AIChE J.*, **37**, 1009-1018, 1991.
22. Samuelsberg A. and B. Hjertager, Computational modeling of gas/particle flow in a riser, *AIChE J.*, **42**, 1536-1546, 1996.
23. Schuegel K., Rheological behavior of fluidized systems, **Fluidization**, Edited by J. F. Davidson and D. Harrison, Academic Press, 1971.
24. Sinclair J. L. and R. Jackson, Gas-particle flow in a vertical pipe with particle-particle interaction, *AIChE J.*, **35**, 1473-1486, 1989.
25. Snook I. & W. van Megen, Machine simulation of colloidal dispersions, **Colloid and Interface Science IV**, Hydrosols and Rheology, Edited by M. Kerker, Academic Press Inc., 1976.
26. Temporally H. N. V., Rowlinson J. S. & Rushbrooke G. S., *Physics of Simple Liquids*, North Holland, 1968.
27. Thiele E. J., equation of state for hard sphere, *J. Chem. Phys.*, **39**, 474-479, 1963.

28. Watts R. O. & I. J. McGee, **Liquid State Chemical Physics**, John Wiley & Sons, Inc., 1976.
29. Wertheim M. S., Exact solution of the Percus-Yevick Integral equation for hard spheres, *Phys. Rev. Lett.*, **10**, 301-323, 1963.
30. Wood W. W., Monto Carlo studies of Simple liquid models, **Physics of Simple Liquids**, Edited by H. N. V. Temperley, J. S. Rowlinson & G. S. Rushbrooke, North Holland, 1968.
31. Yoshida H., K. Ito & N. Ise, Microscopic observation and quasielastic light-scattering measurements of colloid crystals, Determination of the radial distribution function and structure factor for the two-state structure, *J. Am. Chem. Soc.*, **112**, 592-596, 1990.

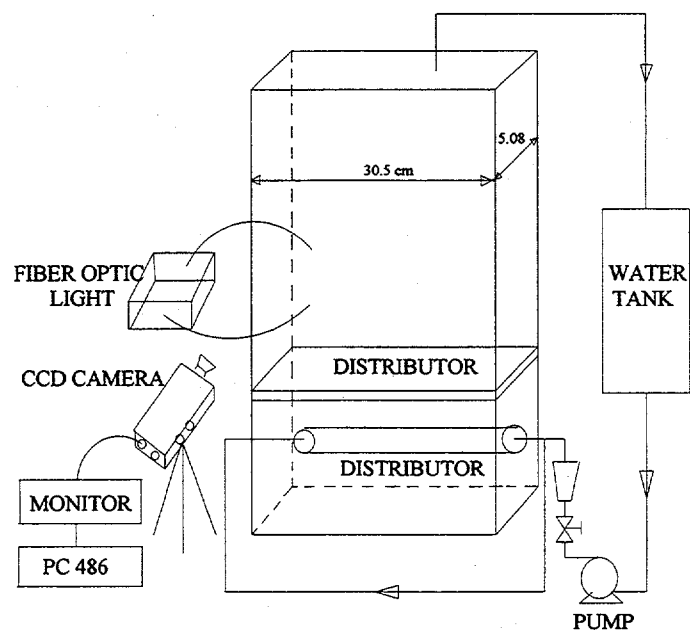


Fig. 1 Liquid-Solid Fluidized Bed With Instruments

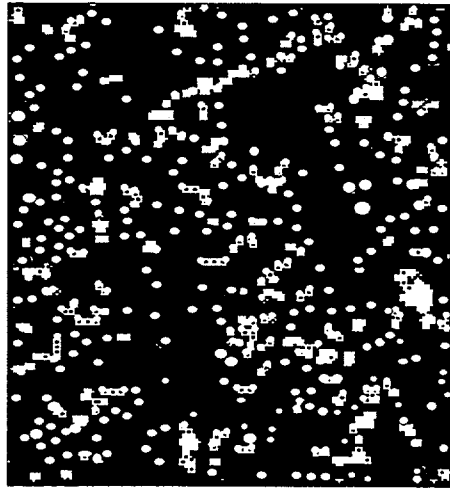
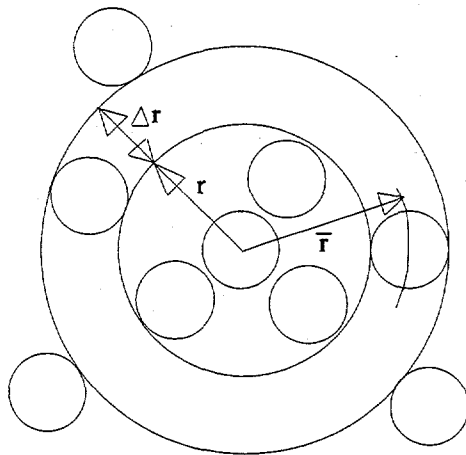


Fig. 2 A Small Portion of Image Captured by
CCD Camera for 450 Micron Galss Particles



particles in shell between r and $r+\Delta r$:

$$\Delta N = 2\pi\bar{r}\left(\frac{N}{\text{AREA}}\right)g(\bar{r})\Delta r$$

where: N is particles number in the observed area. Thus

$$\text{Local Density of Particles} = \left(\frac{N}{\text{AREA}}\right)g(r)$$

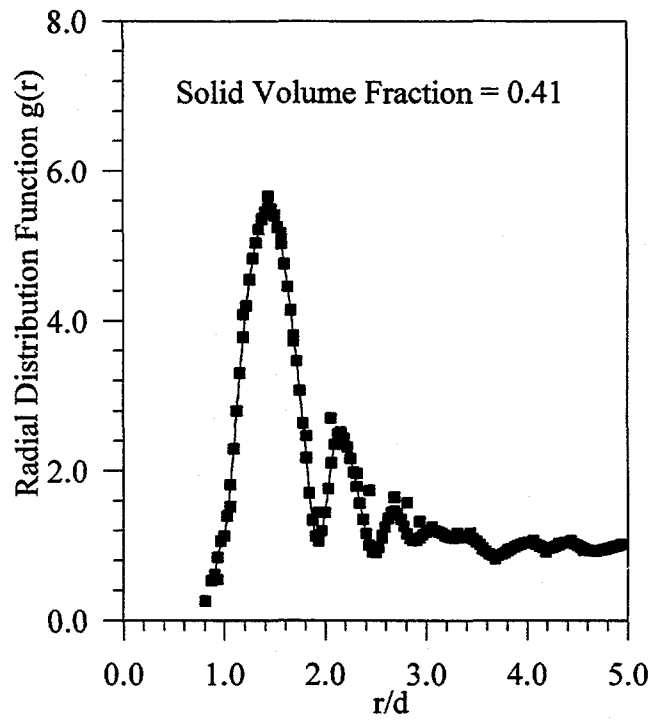
$$\text{where: } r = \sqrt{(x_i - x_j)^2 + (y_i - y_j)^2}$$

To prevent two particles to be at the same location, for $r \leq d$ (particle size), $g(r) = 0$. As

$r \rightarrow \infty$,

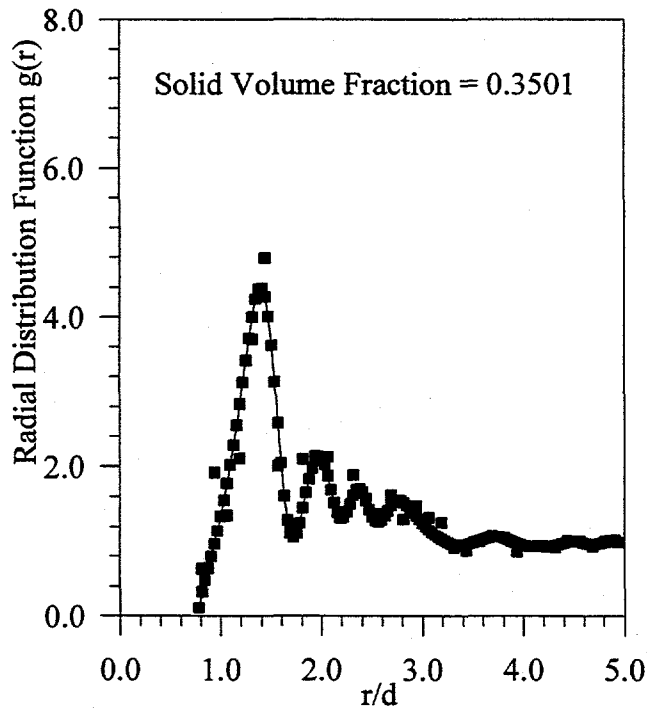
local density = local density $\times g(r)$. Hence, $g(r) \rightarrow 1.0$.

Fig. 3 Concept of Radial Distribution Function



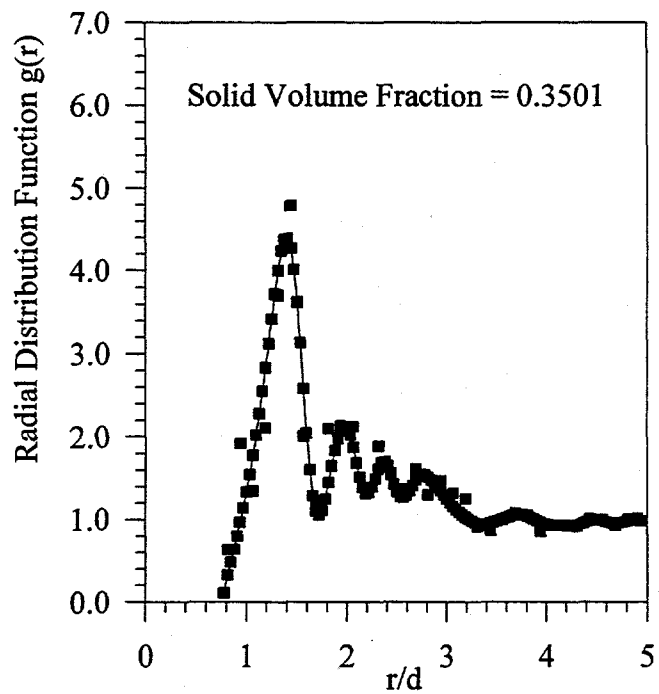
(a)

Fig. 4_a Radial Distribution Function Profile



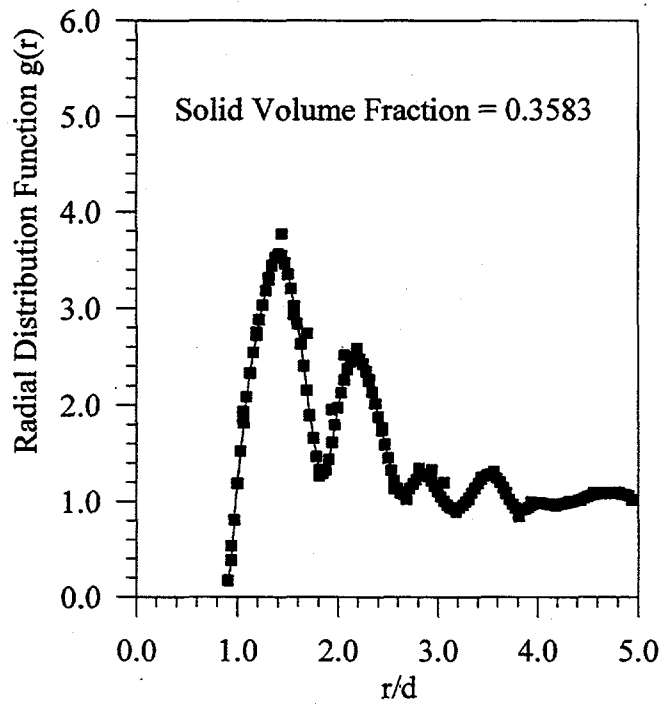
(b)

Fig. 4_b Radial Distribution Function Profile



(c)

Fig. 4_c Radial Distribution Function Profile



(d)

Fig. 4_d Radial Distribution Function Profile

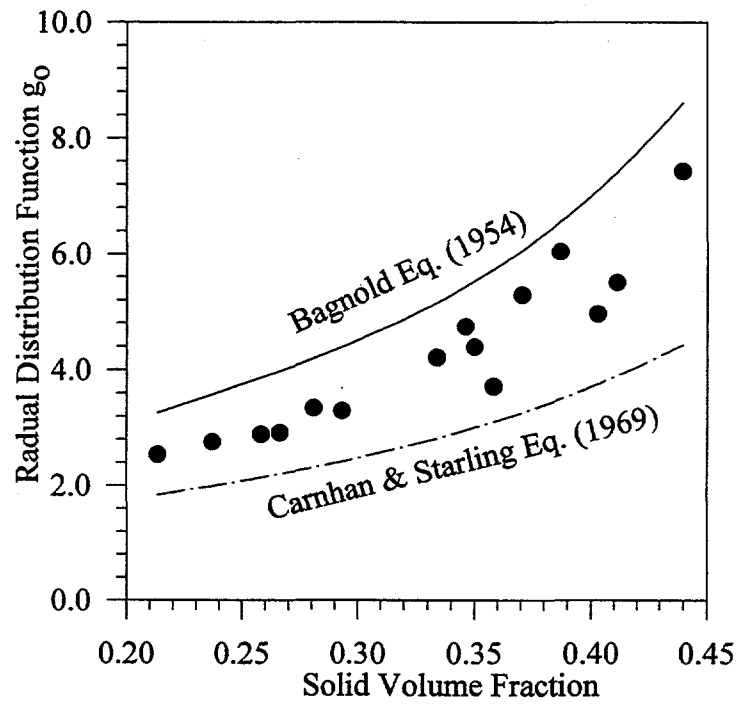
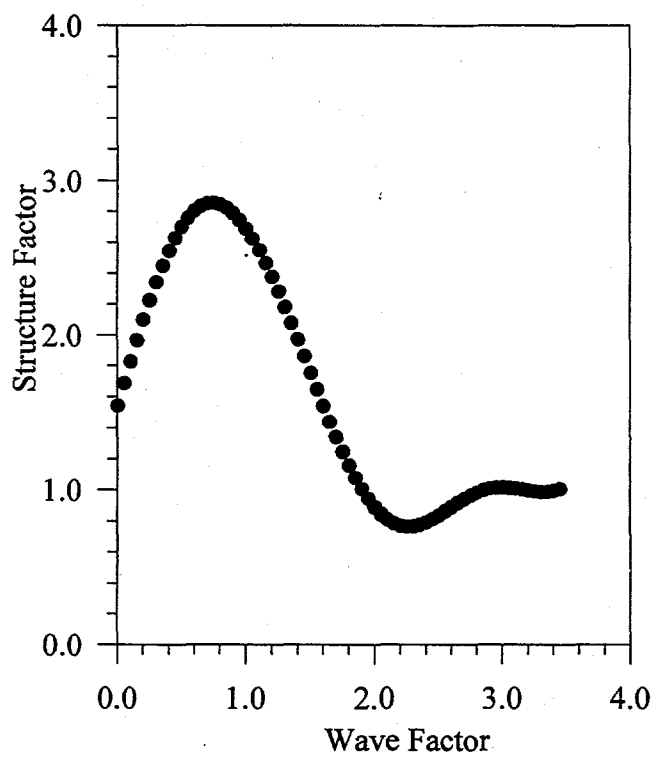
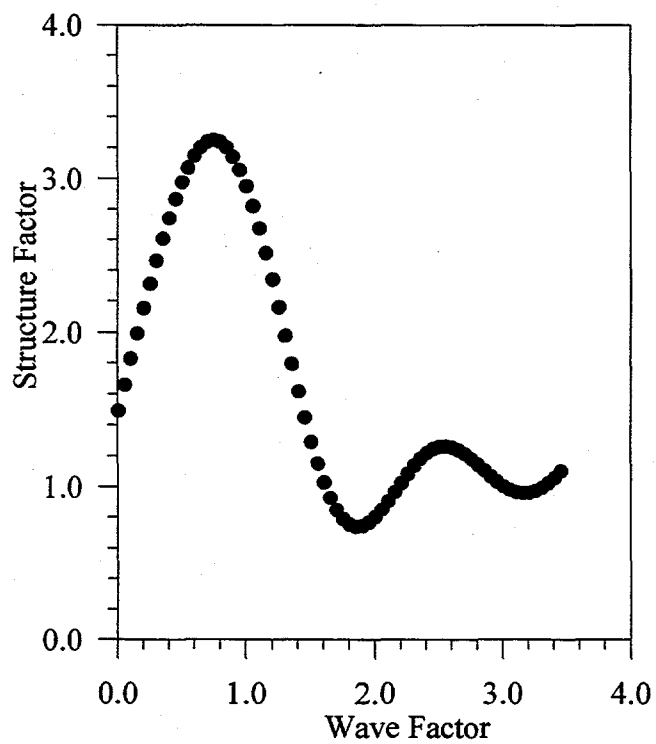


Fig. 5 A Comparison of Measured Radial Distribution Function With Computed Results of Bagnold and Carnahan & Starling Equations



(Solid Volume Fraction = 0.334)

(a)



(Solid Volume Fraction = 0.266)

(b)

Fig. 6 Profiles of Structure Factor Distribution

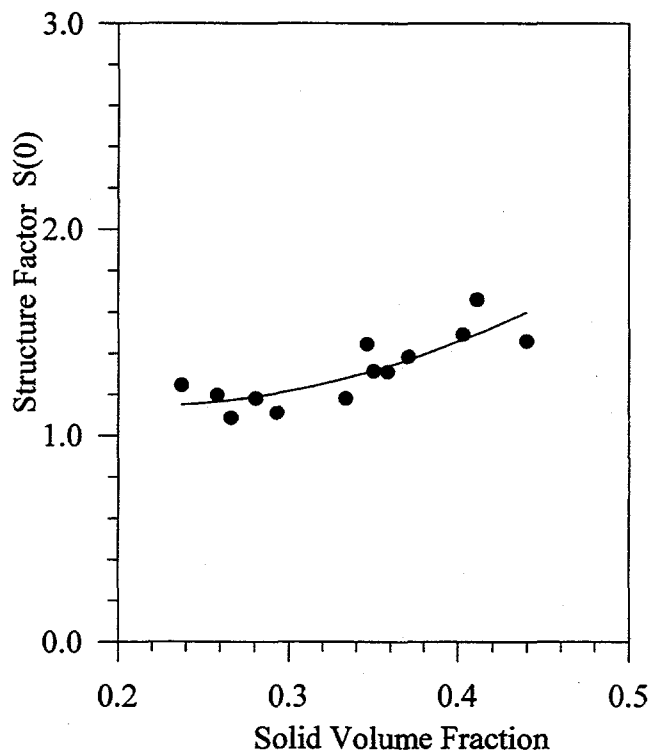


Fig. 7 Structure Factor S(0) Profile

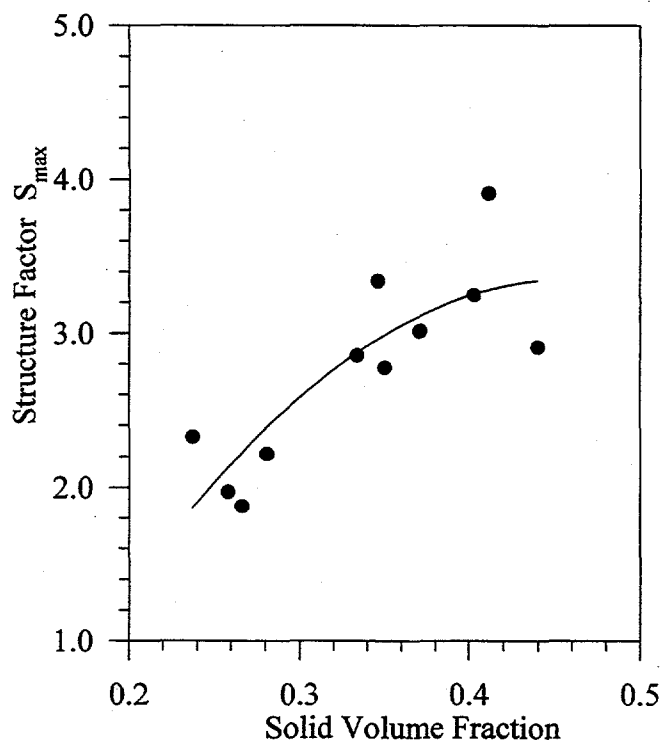
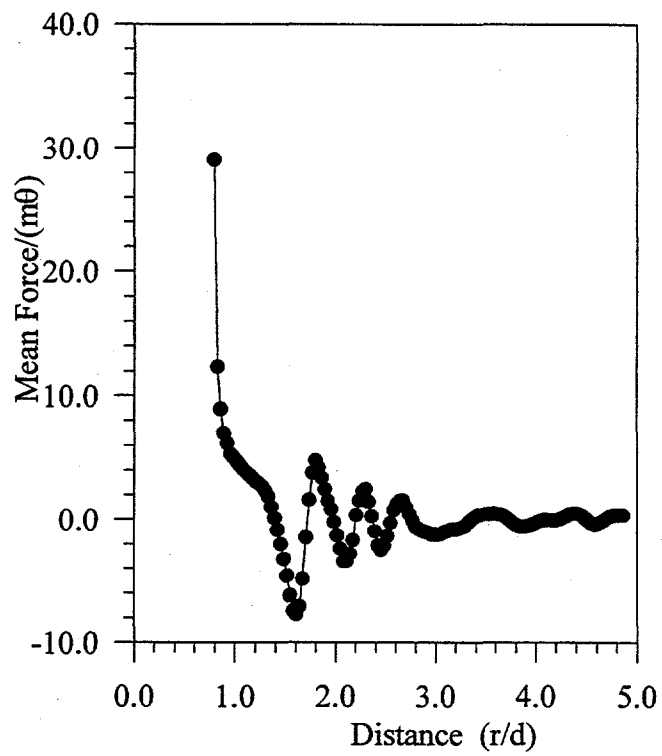
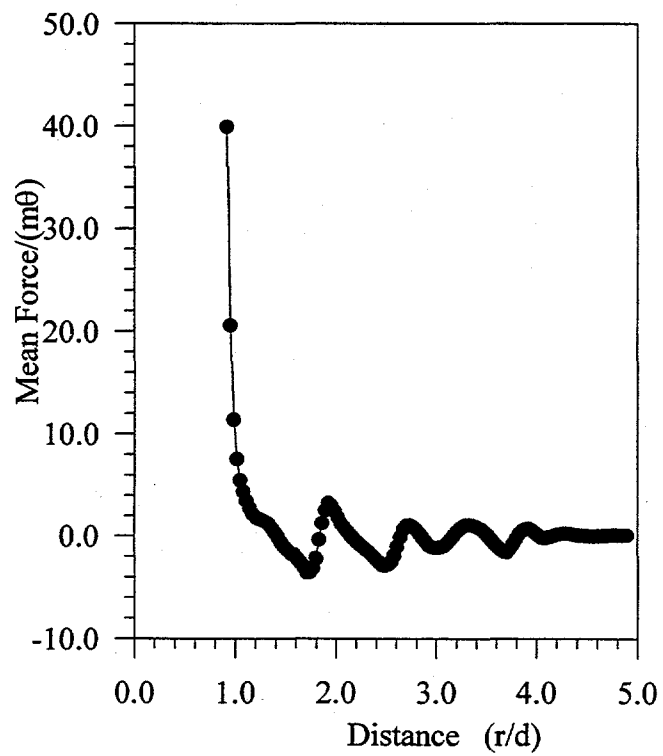


Fig. 8 Major Peak Values of The Structure Factor



(Solid Volume Fraction = 0.3501)

(a)



(Solid Volume Fraction = 0.2931)

(b)

Fig. 9 Profiles of Mean Force Distribution

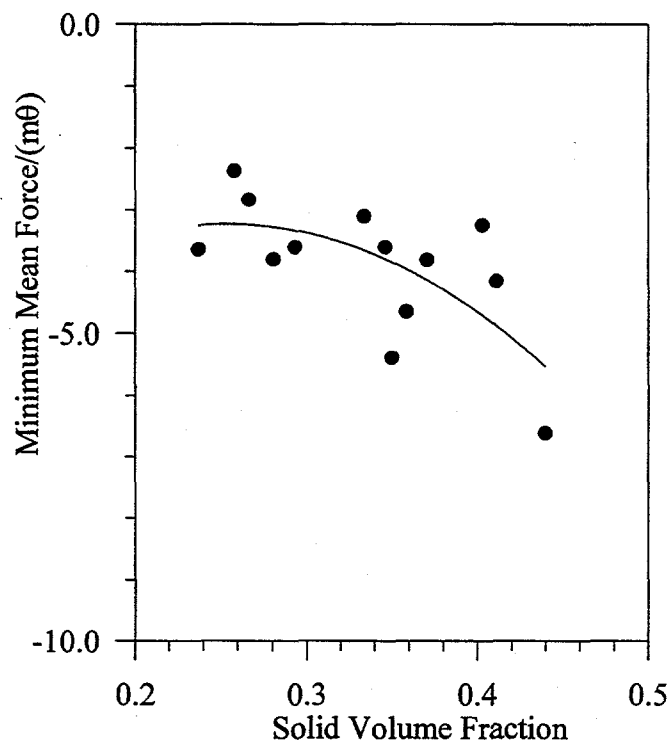
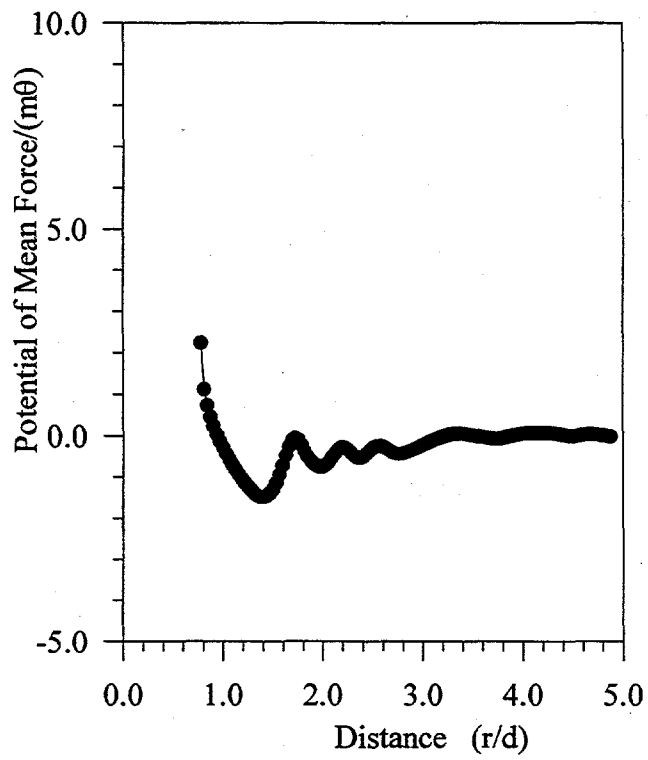
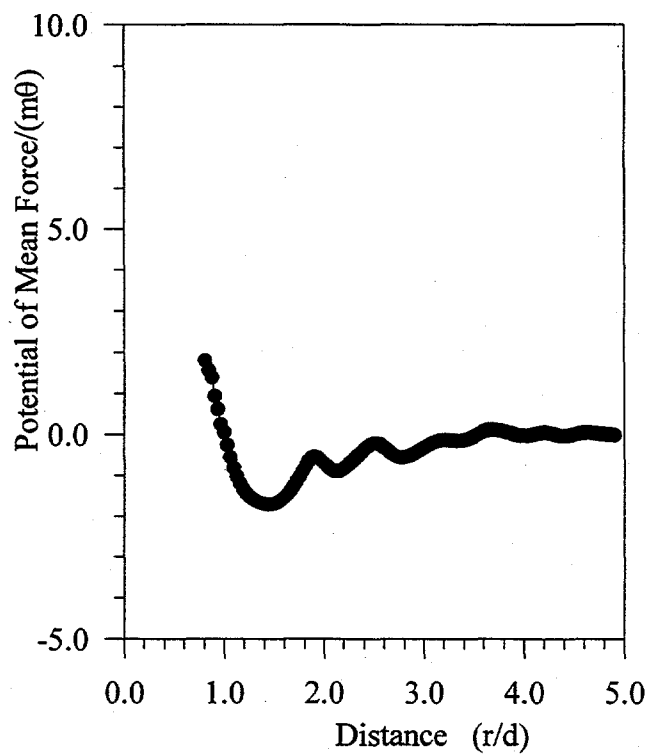


Fig. 10 Minimum Mean Force Distribution Profile



(Solid Volume Fraction = 0.3501)

(a)



(Solid Volume Fraction = 0.4112)

(b)

Fig. 11 Potential of Mean Force Distributions

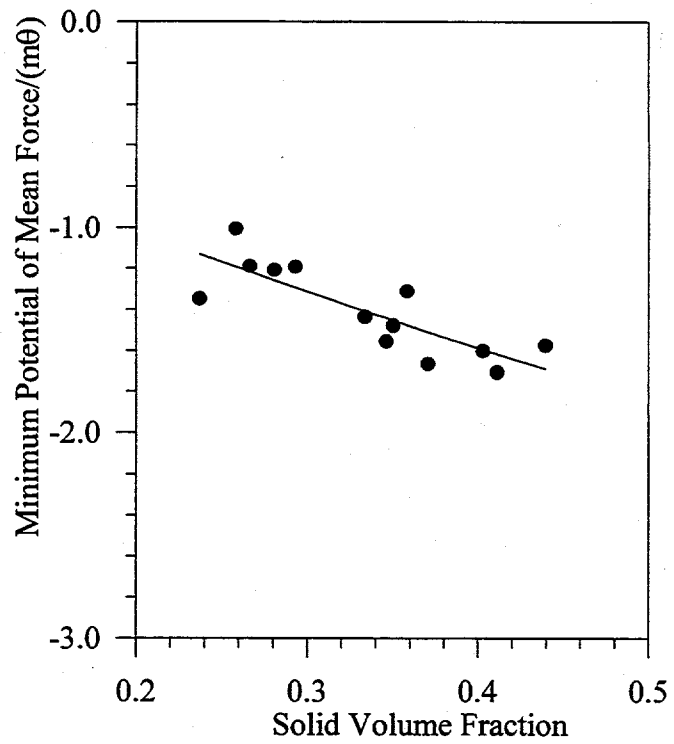


Fig. 12 Minimum Potential of Mean Force Distribution